

Comparative Analysis of Frequency Ratio, Logistic Regression and Deep Learning Methods for Landslide Susceptibility Mapping in Tokat Province on the North Anatolian Fault Zone (Turkey)

Ayhan BAŞALAN^{1*}
Gökhan DEMİR²



ABSTRACT

In the current investigation, a Geographic Information System (GIS) and machine learning-based software were employed to generate and compare landslide susceptibility maps (LSMs) for the city center of Tokat, which is situated within the North Anatolian Fault Zone (NAFZ) in the Central Black Sea Region of Turkey, covering an area of approximately 2003 km². 294 landslides were identified within the study area, with 258 (70%) randomly selected for modeling and the remaining 36 (30%) used for model validation. Three distinct methodologies were used to generate LSMs, namely Frequency Ratio (FR), Logistic Regression (LR), and Deep Learning (DL), using nine parameters, including slope, aspect, curvature, elevation, lithology, rainfall, distance to fault, distance to road, and distance to stream. The susceptibility maps produced in this study were categorized into five classes based on the level of susceptibility, ranging from very low to very high. This study used the area under receiver operating characteristic curve (AUC-ROC), overall accuracy, and precision methods to validate the results of the generated LSMs and compare and evaluate the performance. DL outperformed all validation methods compared to the others. Finally, it is concluded that the generated LSMs will assist decision-makers in mitigating the damage caused by landslides in the study area.

Keywords: Landslide susceptibility, GIS, NAFZ, frequency ratio, logistic regression, deep learning, Turkey.

Note:

- This paper was received on May 1, 2023 and accepted for publication by the Editorial Board on July 19, 2024.
- Discussions on this paper will be accepted by March 31, 2025.
- <https://doi.org/10.18400/tjce.1290125>

1 Tokat Gaziosmanpaşa University, Department of Civil Engineering, Tokat, Türkiye
ayhanbasalan@gmail.com - <https://orcid.org/0000-0002-1342-1336>

2 Ondokuzmayıs University, Department of Civil Engineering, Samsun, Türkiye
gokhandemir61@gmail.com - <https://orcid.org/0000-0002-3734-1496>

* Corresponding author

1. INTRODUCTION

The Earth is a living and dynamic inorganic entity akin to the living organisms that inhabit it. This dynamism of the Earth manifests itself in the form of natural events such as earthquakes, volcanic activity, tsunamis, floods, and landslides. Among these natural events, earthquakes are the most prevalent. It is well-established that landslides often occur as a result of earthquakes. In addition, landslides can be triggered by other natural processes, such as floods, intense and sudden rainfall, sudden changes in temperature, and human disruption of the natural equilibrium. Landslides significantly threaten life and property in regions characterized by steep topography and high precipitation [1, 2]. Landslides, a ubiquitous phenomenon worldwide, significantly impact the environment and economy in Turkey, particularly in densely populated residential areas, resulting in the loss of life and property. The recurrence and escalation of landslides into natural disasters in Turkey can be attributed to a combination of geological, climatic, and geographical factors and inadequate land management practices. In particular, the Eastern Black Sea region experiences intense landslides with devastating consequences [3]. Given the destructive nature of landslides, identifying and mapping landslide-prone areas is crucial for preventing losses. To this end, various studies, including the production of landslide hazard, risk, and susceptibility maps, have been conducted by researchers to identify and mitigate the potential consequences of landslides [4, 5, 6, 7, 8, 9]. Landslide hazard maps are cartographic representations that assess the probability of landslide occurrence in a specific location, accounting for spatial, temporal, and size-related factors. According to scholars, a practical landslide hazard map should encompass a comprehensive inventory assessment, a thorough analysis of the factors that lead to and trigger landslides, their spatial distribution, and information on their probability, nature, and magnitude [5, 10]. In addition, landslide risk maps comprise assessments of probable losses and destruction and financial and ecological consequences. To create accurate landslide hazard maps, it is necessary to have detailed information on the population, settlement, and economic conditions of the region. The production of such maps requires the expertise of experts from both social and natural sciences, as well as a multidisciplinary approach to planning and research [3, 11]. In addition, sensitivity maps are necessary for creating hazard and risk maps [12, 13]. LSMs are thematic representations that classify the relative susceptibility of areas to landslides in the future, considering factors that are believed to play a role in landslide formation in a specific location. In LSMs, research areas are typically divided into five classes of susceptibility, ranging from very low to very high [14, 15, 16]. In recent years, the study of landslide susceptibility has gained significance because it serves as a means of minimizing the damage caused by landslides and providing guidance for land-use planning [5, 17]. Advances in GIS, remote sensing techniques, computer technology, and software have enabled the storage and statistical analysis of large amounts of data, leading to increased use of artificial intelligence and non-empirical statistical methods in landslide susceptibility assessments. These studies are precious for disaster prevention and mitigation [18, 19]. Furthermore, the prevalence of these studies has increased in recent years because of technological advancements, which suggests a higher level of sophistication in this field. This study aimed to generate and contrast high-resolution LSMs of Tokat province, which is located in the North Anatolian Fault Zone (NAFZ), by employing FR, LR, and DL techniques in a GIS environment. The absence of previous research on landslide susceptibility mapping in the provincial center of Tokat and the area's location within the NAFZ provided the impetus for this study to be conducted in the region.

2. STUDY AREA

The Turkish province of Tokat is geographically situated within the Central Black Sea Region on the NAFZ, a seismically active zone that is notorious for frequently generating devastating earthquakes. The population of the central district of Tokat, which includes 12 districts, including the city center, was recorded as 204.907 in 2022 [20]. The topography of the provincial capital is characterized by cliffs and hills in the east-west direction and mountains and hills with gentle slopes in the north direction. The district center of the province, which spans an area of approximately 2003 km², is located between 36°25' and 37°00' east longitude and 39°55' and 40°35' north latitude (Figure 1). Tokat is a transitional climate between the Black Sea and Central Anatolian steppe. While the northern regions of the study area exhibit the characteristics of the Black Sea climate, the southern regions display the characteristics of the Central Anatolian Steppe. The elevation of the study area above sea level ranged between 585 m and 2079 m, and the maximum slope value was recorded as 80.3°. The Yeşilirmak River traverses the study area, and landslides in the region can be induced by factors such as unanticipated earthquakes, anthropogenic activities, changes in groundwater level, or a combination of these factors. Field observations have shown that landslides predominantly occur in thick, weathered topsoil areas.

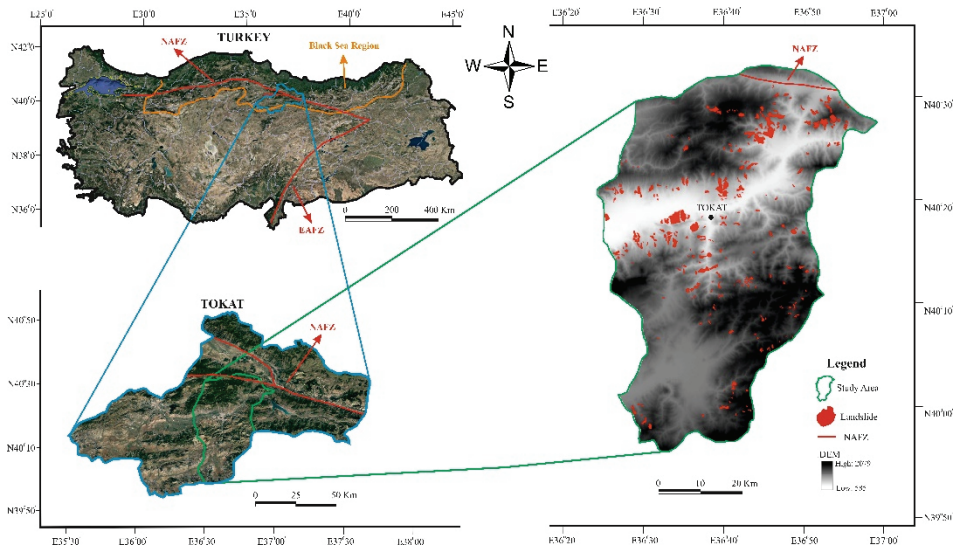


Figure 1 - Location map of the study area

3. MATERIALS AND METHODS

The process of assessing landslide susceptibility is highly dependent on the compilation of reliable and relevant data and parameters related to landslides in the study area. Thus, any errors or deficiencies in the data and parameters used can significantly affect the accuracy of the resultant LSMs [13, 21]. Several techniques have been developed in recent years to create landslide susceptibility and hazard maps using statistical models and GIS tools. Some studies have used statistical models such as logistic regression, bivariate and multivariate analysis,

and probabilistic models such as frequency ratio and weight of evidence. In addition, other approaches, including analytical hierarchy process, index of entropy model, certainty factor model, artificial neural network model, spatial multicriteria decision analysis approach, fuzzy logic and neuro-fuzzy, deep learning, decision-tree methods, and support vector machine model have been applied for landslide susceptibility mapping [22, 23, 24, 25, 26, 27]. Previous research on landslide susceptibility mapping was reviewed as part of this study to inform the selection of relevant data and parameters [19, 24]. This review comprehensively discusses the data, parameters, and methodologies integral to creating LSMs [28, 29, 30]. The present study adopted a combined approach incorporating the widely used FR and LR statistical techniques and the DL machine learning algorithm to produce LSMs. A schematic representation of the methodology used in this study is shown in Figure 2. This flowchart shows the sequence of procedures and processes used throughout the study.

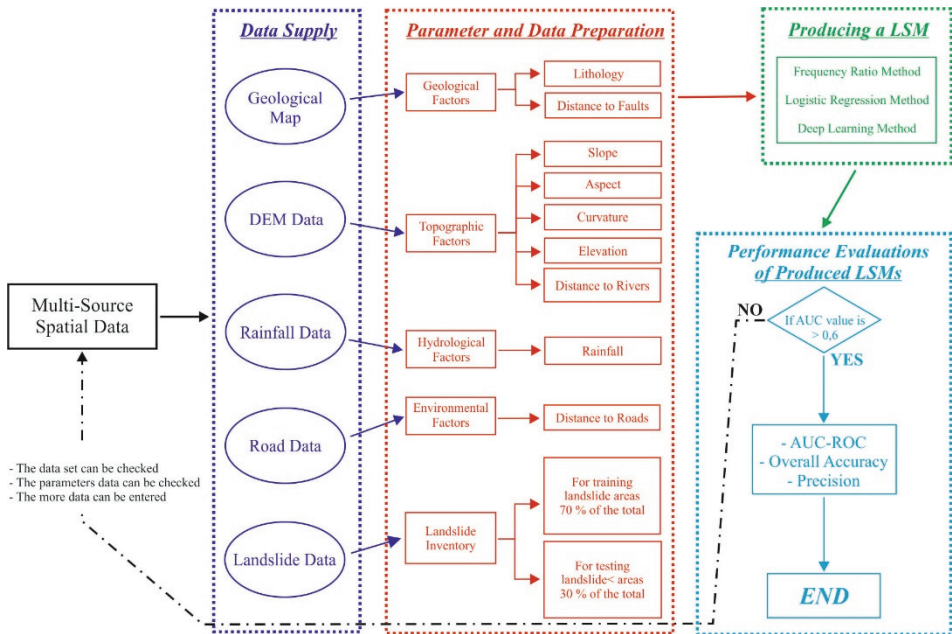


Figure 2 - Workflow chart of the study

3.1. Landslide Inventory

Landslide inventory maps represent the location of landslides, typically containing details on the type, date, and location of landslides [24]. These maps are crucial for creating accurate inventory, landslide, hazard, and risk maps. Compiling a comprehensive landslide inventory is essential in evaluating previous landslide assessment maps [31]. Various sources, such as literature, field studies, digital maps, aerial photographs, and satellite images, can be used to gather information for the landslide inventory. In the present research, a combination of field investigations (Figure 3a, 3b, 3c, and 3d), aerial photographs (Figure 3e, 3f, and 3g), and printed and digital maps developed by the Mineral Research and Exploration Department were employed to acquire the landslide inventory for the study region [32]. Because of the

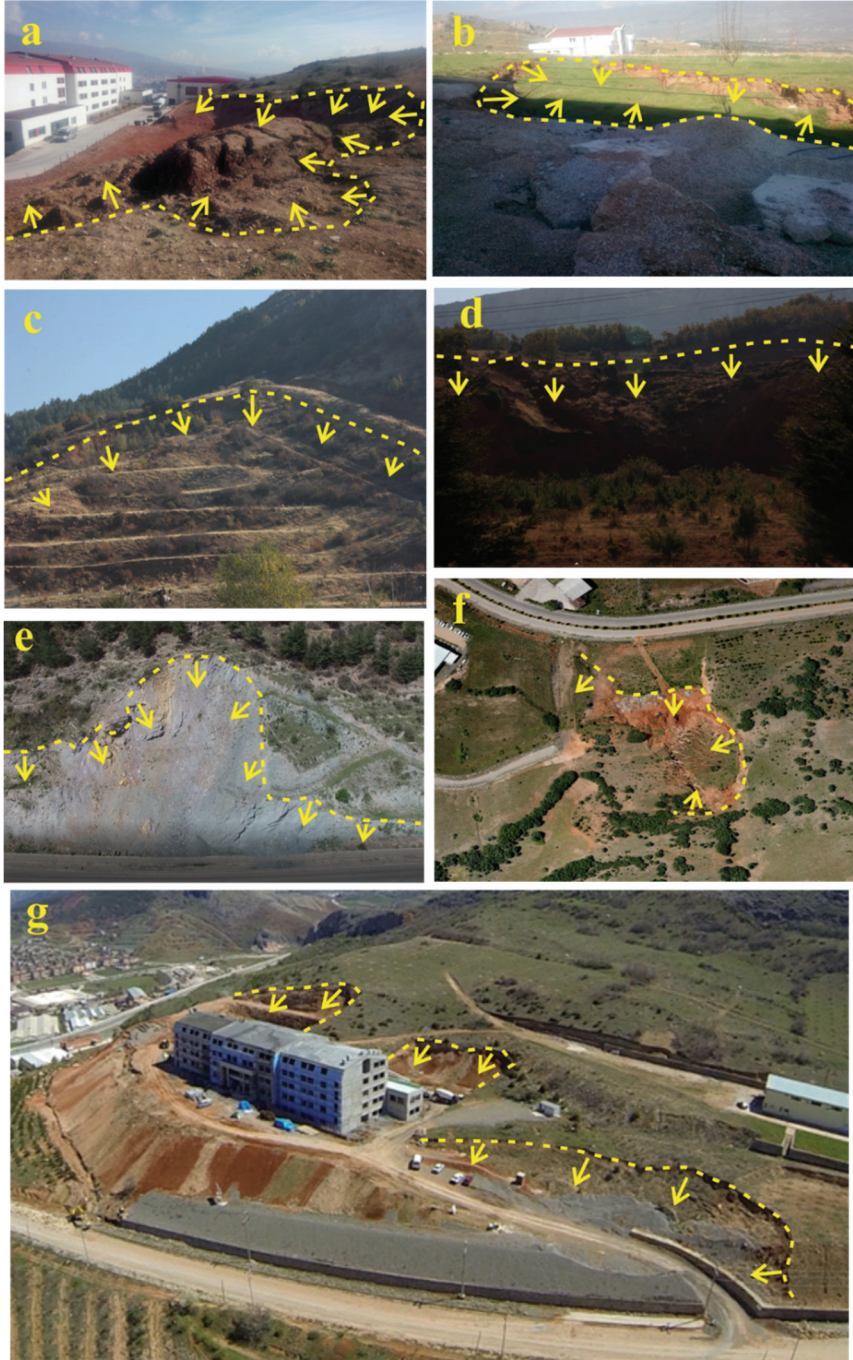


Figure 3 - Images of some landslides in the study area: a, b, c, and d images, e, f, and g aerial images (arrows show the direction of movement of landslides)

collection of historical landslide data, interpretation of remote sensing images, and field survey, 294 landslides were identified within the study area (Figure 4). According to the data, these 294 landslide areas comprise 482.649 pixels (12.5 m x 12.5 m) and cover approximately 3.76% of the study area. Approximately 70% of the landslide areas (314.019 pixels) were used for analysis in the applications, whereas the remaining 30% (141.630 pixels) were used to test the performance of the generated landslide susceptibility models. The landslides allocated for analysis and performance testing were chosen at random.

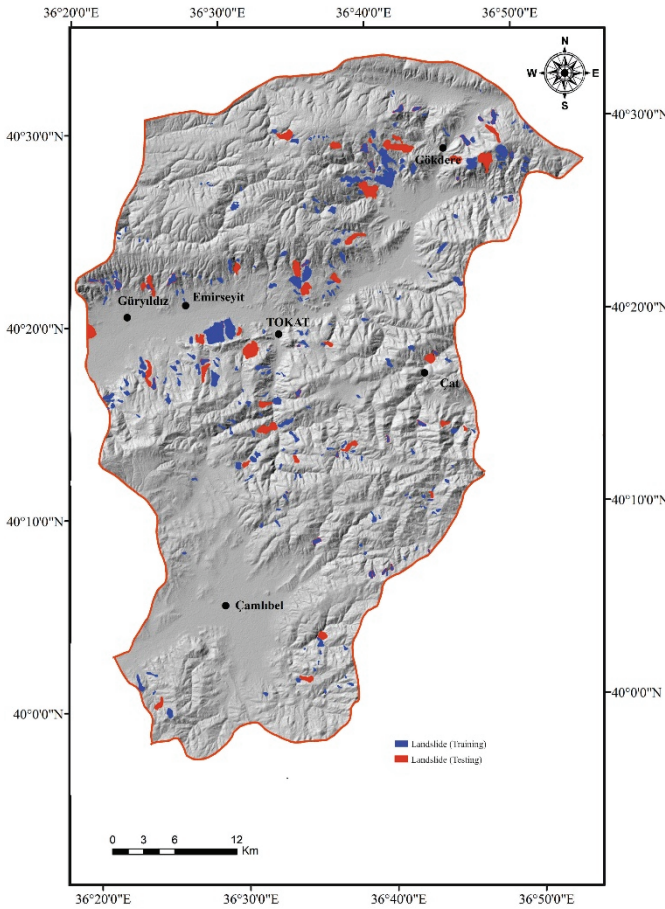


Figure 4 - Landslide inventory map of the study area

3.2. Data Preparation

Determining factors affecting landslides is mainly driven by their significance to the incidence of landslides in a particular region and the accessibility of related data [17, 33]. The factors chosen for GIS-based research should be operational, comprehensive, irregular, measurable, and non-redundant [15, 34, 35]. This study produced nine data layers based on a review of relevant literature and field investigations to identify the significant factors

influencing landslide occurrences within the study area. The generated data layers included slope, aspect, curvature, elevation, rainfall, lithology, distance to faults, distance to roads, and distance to streams (Figure 5). The slope is one of the most critical parameters in forming landslides because of its high level of influence and ease of mapping [36, 37, 38]. Researchers often use slope as a parameter for generating LSMs. The slope is defined as the angle of inclination of a surface relative to the horizontal plane, expressed in degrees [39]. Alterations in the slope and the destabilization of materials on a slope are considered the most fundamental factors leading to landslides [7]. Nine distinct slope categories ranging from 0° to 80.3° were established for the study area, and it was observed that most slopes fell within the 0° to 30° range (Figure 5a). The parameter aspect holds significant importance in landslide susceptibility research, as it denotes the orientation of the land surface and can be characterized by the direction of the tangent plane at any given location on the surface [40, 41]. In the study area, the values of the aspect were segregated into nine distinct directional categories. The study area had the most significant percentage of area facing the east direction, 12.68%, and the most minor area facing the north direction, 9.76% (Figure 5b). Curvature, defined as the rate at which the angle or direction of the land slope changes in a particular, is found to reach high and wide-range values in narrow areas [34]. The map depicting the curvature of the study area was categorized into three classes: flat, concave, and convex. A significant proportion of the study area was classified as concave (34.47%), followed by convex (33.77%), and flat (31.76%) (Figure 5c). Elevation, another commonly used parameter in landslide susceptibility studies [16, 42, 43], was found to vary between 575 m and 2079 m in the study area. It has been observed that landslides occur at almost all elevation values but with a higher concentration between 755 m and 1410 m (Figure 5d). Rainfall is widely recognized as a trigger for landslides on slopes [44, 45]. The annual average rainfall values in the study area vary between 765 and 1115 mm. It has been observed that landslides occur at almost all rainfall values, with a higher concentration observed between 765 mm and 899 mm (Figure 5e). The lithology parameter, which refers to the physical properties of rock units such as color, texture, and grain size, is commonly used in landslide susceptibility studies [46, 47, 48]. In this study area, lithology classes were divided into eight different classes, and landslides were observed in all units except the alluvial unit. It was also observed that most landslide areas were concentrated in the Tokat metamorphics (Pztm) and Haydaroğlu formation (Teh) (Figure 5f). In the landslide susceptibility analysis, the distance from faults is a crucial parameter. This is because such proximity may result in rock fragmentation, adversely impacting slope stability [49, 50]. Structural elements can weaken the surrounding materials and increase the likelihood of landslides. Similarly, proximity to roads is also considered a significant factor in landslide susceptibility analysis, as they can cause loss of heel support or additional load on sensitive slopes [23, 51, 52, 53, 54]. The degree of saturation of slopes, which is determined by the distance between slopes and streams, is a critical factor in landslides [33]. Therefore, the distance to faults, roads, and streams are deemed significant parameters in evaluating landslide susceptibility and are commonly referred to as stream density, distance to the drainage network, and drainage density [55]. Buffer analysis created maps for these parameters at 100 m intervals. According to the obtained data, it has been observed that landslide areas are concentrated in areas farther than 900 meters away from the three parameters mentioned above (Figure 5g, 5h, and 5i).

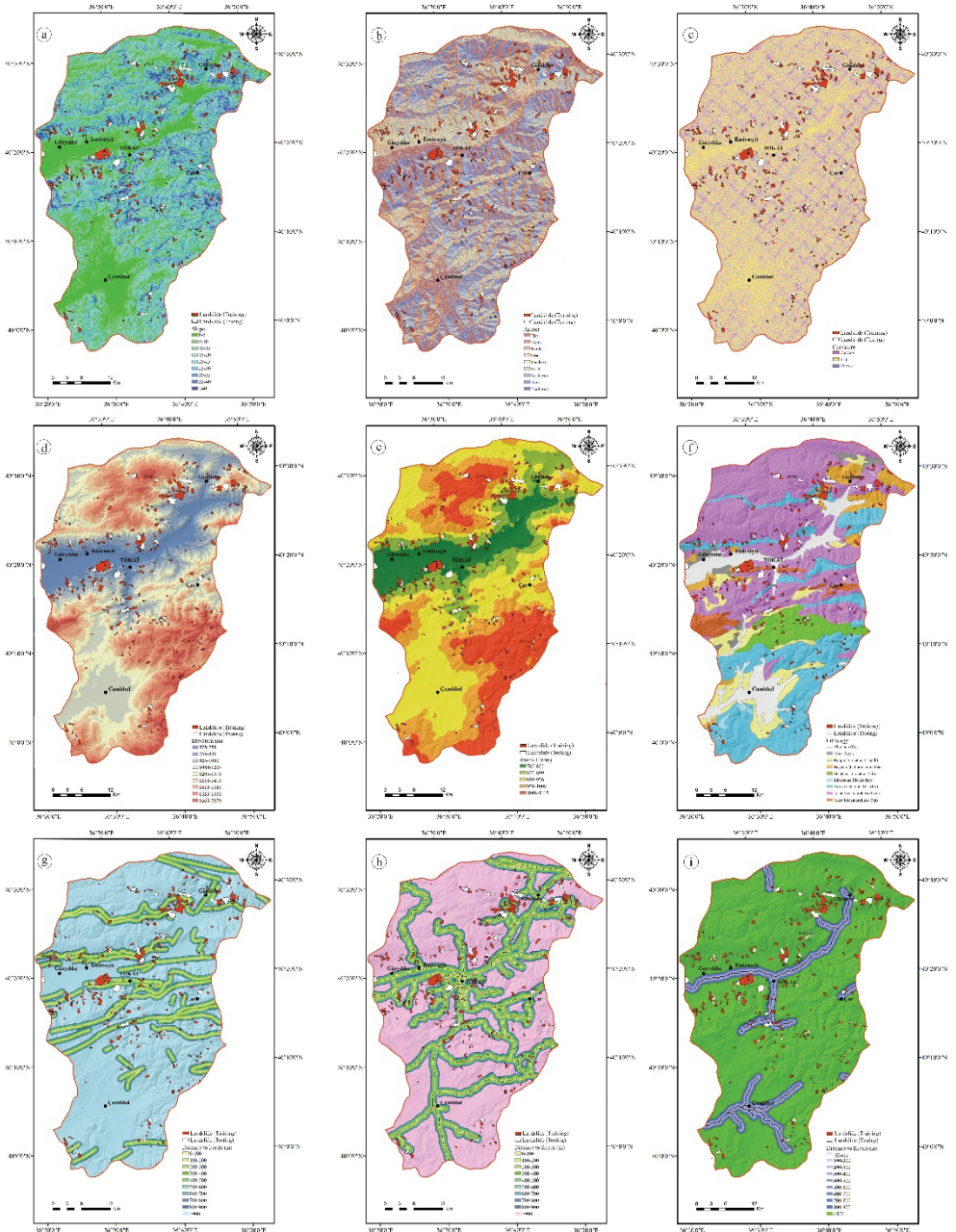


Figure 5 - Landslide conditioning factors: (a) slope, (b) aspect, (c) curvature, (d) elevation, (e) rainfall, (f) lithology, (g) distance to faults, (h) distance to roads and (i) distance to streams

3.3. Landslide Susceptibility Assessment Methods

This study employed FR, LR, and DL methods for landslide susceptibility assessment.

3.3.1. Frequency Ratio Method

The FR method, which computes the observation frequency of parameter sublayers within landslide zones, facilitates the objective weighting of parameter maps and their respective sublayers while estimating areas prone to landslide susceptibility. Using the FR method, the sublayers of parameter maps within the study area can be correlated with the sublayers of actual landslide areas. This approach relies on a probability model that evaluates the likelihood of a particular event occurring [56, 57, 58, 59]. The following is the formula for this method (Eq. 1);

$$FR = \frac{PLO}{PIF}, \quad (1)$$

PLO refers to the percentage of each substrate affecting landslides in the formula, and PIF refers to the percentage of each substrate causing landslides in the parameter map. The parameter maps were assigned weights based on the FR determined using the above formula [60, 61].

The summation of the frequency ratio values belonging to each factor category was used to calculate the landslide susceptibility index (LSI), as expressed in equation 2;

$$LSI = \sum_{i=1}^n FR, \quad (2)$$

Because of reclassifying the LSI map using the equal interval methodology in GIS, the study region was partitioned into five susceptibility categories: very low, low, moderate, high, and very high. Weighted parameter maps were generated by assigning lower values to areas with lower landslide susceptibility and higher values to regions with higher susceptibility. These maps were then combined to produce an LSM. To determine the final state of the LSM, these values were grouped into classes of equal intervals [62].

3.3.2. Logistic Regression Method

Regression analysis is a statistical method that involves explaining or understanding a variable based on one or more other variables. The variable being explained is referred to as the dependent or response variable, while the different variables used to predict or explain the response are known as independent variables or predictors. LR is a statistical technique that researchers and statisticians extensively employ for analyzing binary and proportional response data [63]. In the production of LSMs, LR, a multiple logistic regression method, is commonly used [64]. LR permits the development of a multivariate regression model that establishes a relationship between a dependent variable and multiple independent variables. The dependent variable can be binary, whereas the independent variables may assume

interval, binary, or categorical forms [65, 66]. When performing the LR analysis, the numerical values of the dependent variable should be 0 or 1. The LR coefficients obtained from the analysis can be used to generate independent variables. The relationship between the data in the LR analysis is expressed by the formula provided below [23, 66, 67];

$$p = \frac{1}{(1+e^{-z})} = \frac{e^z}{1+e^z} \quad (3)$$

In the formula, the symbol 'p' represents the probability of a landslide occurrence, which assumes the form of an S-shaped curve ranging from 0 to 1. This probability is estimated using LR;

$$z = \beta_0 + \beta_1x_1 + \beta_2x_2 + \dots + \beta_n \quad (4)$$

and the equation, as mentioned above, yields the value of 'z'. In this equation, β_0 represents the model constant value, $\beta_1, \beta_2, \dots, \beta_n$ represent the coefficients of the independent variables, and x_1, x_2, \dots, x_n are the independent variables. The equation's dependent variable 'z' corresponds to the landslide condition. The model reveals a landslide (1) and no landslide (0) on the independent variables of the landslide.

3.3.3. Deep Learning Method

DL is a subfield of machine learning that leverages multi-layered data representations, commonly using artificial neural networks, to attain cutting-edge performance in tasks such as image classification, object detection, speech recognition, and document classification [68]. DL incorporates self-learning artificial neural networks, called deep learning neural networks (DNNs) or stacked artificial neural networks [69], to process and analyze data through multiple layers. The depth of these networks, represented by the number of hidden layers, distinguishes DNNs from other types of neural networks, such as multi-layer perceptron networks. The complexity of DNNs is characterized by the intricate patterns in which information flows throughout the network, as evidenced by the increasing number of hidden layers and nodes in more advanced architectures. Despite this complexity, the fundamental concept of DNNs remains unchanged. Deep neural networks (DNNs) possess a unique characteristic known as feature hierarchy, a hierarchical structure of increasing complexity and abstraction. This feature enables DNNs to handle vast, high-dimensional datasets with billions of parameters passing through nonlinear functions. As a result, unlike traditional machine learning algorithms, DNNs can perform automatic feature extraction without human intervention. Given that feature extraction is a task that can take years for data scientist teams to accomplish, DNNs provide a means to circumvent the bottleneck of limited expertise and enhance the capabilities of small data science teams, which inherently do not scale. Over time, various types of neural networks have been developed, such as convolutional neural networks (CNNs) and recurrent neural networks (RNNs), which are thought to emulate the human visual system and interpret sequential data. Despite their complexity, these networks can be considered variations of the same concept, as evidenced by the fact that all types of neural networks can use the same learning algorithms, such as

gradient descent using backpropagation [70, 71, 72]. The present research uses the obtained data to employ a deep neural network (DNN) architecture for text classification.

3.3.3.1. Deep neural Networks (DNN)

The networks used in this system are similar to the human brain's neurons (Figure 6). When a stimulus is presented, the networks undergo a process. The networks can be connected and signed or unconnected and unsigned but are generally organized into layers. To perform a task, the network system must process data through the layers between the input and output. The depth of the network, or the number of layers required for processing, increases with the complexity of the task. A deep neural network is beneficial when it is necessary to replace human labor with autonomous processes without compromising efficiency. These types of networks have several real-world applications across various fields [70, 71, 72, 73].

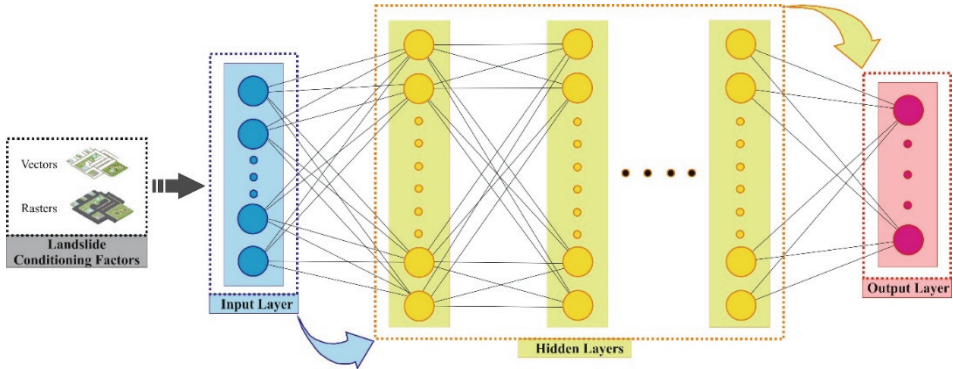


Figure 6 - DL architecture

4. RESULTS

4.1. Results of the Frequency Ratio Method

The frequency ratio value represents the degree of association between the incidence of landslides and the factors under consideration. After creating maps for all the analyzed parameters, the FR formula was used to determine the FR values for the sublayers of each parameter. The data obtained for the sublayers are tabulated in Table 1 and presented visually.

Table 1 - Frequency ratio analysis of landslide conditioning factors

Parameters	Pixel Number of Total Areas	Ratio (% PIF)	Pixel Number of Landslide Areas	Ratio (% PLO)	FR % (PLO/PIF)
Slope (°)	0-5	1.783.389	16.991	4,98	0,359
	5-10	2.104.818	51.534	15,11	0,921
	10-15	1.941.286	59.845	17,55	1,161

Comparative Analysis of Frequency Ratio, Logistic Regression and Deep Learning ...

	15-20	2.161.598	16,84	66.239	19,42	1,153
	20-25	1.834.237	14,29	56.117	16,46	1,152
	25-30	1.371.765	10,69	41.253	12,1	1,132
	30-35	9483.59	7,39	28.170	8,26	1,118
	35-40	524.359	4,08	15.804	4,63	1,135
	>40	167.209	1,30	5.065	1,49	1,146
Aspect						
	Flat	1.508.203	11,75	31.152	9,13	0,777
	North	1.252.408	9,76	36.161	10,60	1,086
	Northeast	1.274.841	9,93	37.461	10,99	1,107
	East	1.627.760	12,68	47.100	13,81	1,089
	Southeast	1.535.651	11,96	43.477	12,75	1,066
	South	1.434.310	11,17	37.957	11,13	0,996
	Southwest	1.325.321	10,32	33.118	9,71	0,941
	West	1.533.674	11,95	39.712	11,65	0,975
	Northwest	1.344.852	10,48	34.880	10,23	0,976
Curvature						
	Concave	2.637.812	20,55	74.056	21,72	1,057
	Flat	7.529.587	58,66	192.899	56,57	0,964
	Convex	2.669.621	20,80	74.064	21,72	1,044
Elevation (m)						
	585-755	1.181.322	9,20	27.549	8,08	0,878
	755-925	1.080.062	8,41	72.923	21,38	2,542
	925-1080	1.161.953	9,05	76.338	22,39	2,474
	1080-1205	2.168.970	16,90	52.517	15,40	0,911
	1205-1310	2.038.691	15,88	35.687	10,46	0,659
	1310-1410	1.702.050	13,26	34.597	10,15	0,765
	1410-1535	1.494.245	11,64	18.123	5,31	0,456
	1535-1665	1.423.232	11,09	13.219	3,88	0,350
	1665-2079	586.495	4,57	10.066	2,95	0,646
Rainfall (mm)						
	765-832	1.634.940	12,74	55.027	16,14	1,267
	832-899	1.769.073	13,78	121.075	35,50	2,576
	899-956	4.109.114	32,01	86.352	25,32	0,791
	956-1008	2.782.311	21,67	46.057	13,51	0,623
	1008-1115	2.541.582	19,80	32.508	9,53	0,481
Lithology						
	Qal	1.295.659	10,09	0	0	0
	Teh	715.302	5,57	64.139	18,81	3,377
	Tmplb	936.363	7,29	12.689	3,72	0,510
	Qym	215.382	1,68	602	0,18	0,107

Kb	69.8017	5,44	18.741	5,50	1,011
Ka	3.172.178	24,71	81.432	23,88	0,966
Pz _{tm}	5.420.494	42,23	153.683	45,07	1,067
Pz _t	383.625	2,99	9.733	2,85	0,953
Distance to faults (m)					
0-100	436.276	3,40	21.707	6,37	1,874
100-200	441.502	3,44	20.452	6,00	1,744
200-300	445.504	3,47	18.736	5,49	1,582
300-400	440.711	3,43	17.660	5,18	1,510
400-500	416.917	3,25	15.148	4,44	1,366
500-600	390.348	3,04	13.681	4,01	1,319
600-700	372.137	2,90	12.708	3,73	1,286
700-800	359.890	2,80	12.458	3,65	1,304
800-900	350.501	2,73	13.034	3,82	1,399
>900	9.183.234	71,54	195.434	57,31	0,801
Distance to roads (m)					
0-100	731.747	5,70	22.022	6,46	1,133
100-200	658.299	5,13	19.442	5,70	1,111
200-300	618.216	4,82	18.064	5,30	1,100
300-400	586.494	4,57	17.033	4,99	1,092
400-500	559.658	4,36	17.782	5,21	1,195
500-600	534.901	4,17	17.492	5,13	1,230
600-700	508.530	3,96	17.055	5,00	1,263
700-800	485981	3,79	15.917	4,67	1,232
800-900	465.282	3,62	13.976	4,10	1,133
>900	7.687.912	59,89	182.236	53,44	0,892
Distance to streams (m)					
0-100	195.815	1,53	931	0,27	0,176
100-200	189.891	1,48	1.458	0,43	0,291
200-300	185.427	1,44	2.090	0,61	0,424
300-400	180.924	1,41	2.444	0,72	0,511
400-500	177.600	1,38	2.676	0,78	0,565
500-600	176.103	1,37	2.498	0,73	0,533
600-700	175.520	1,37	2.689	0,79	0,577
700-800	175.228	1,37	3.010	0,88	0,642
800-900	175.167	1,36	3.252	0,95	0,699
>900	11.205.345	87,29	31.9971	93,83	1,075

The study area exhibits high occurrences of landslides in slope classes between 5° and 25°. Lower slope classes are generally expected to have lower landslide frequencies because of reduced shear stresses. The gentle slopes of the study area may be susceptible to landslides

because of the rapid melting of snow. An analysis of the slope aspect reveals that slopes facing east and southeast are particularly vulnerable to frequent landslides. Flat areas experience high landslide frequencies in terms of curvature, while the intensity of landslides is highest between 755 and 1080 m elevation, followed by 1205 to 1410 m elevation. Precipitation falling in the 832-956 mm range is associated with high landslide intensity. The evaluation of distances to faults, rivers, and roads indicates that distances exceeding 900 m significantly correlate with landslide occurrence. After the computation of FR values, the parameter maps underwent reclassification within the GIS software using its corresponding modules. This results in the generation of updated classified parameter maps. The Raster Calculator process was used to create a novel LSM. After its creation, the map, as mentioned above, was subjected to a reclassification process, ultimately resulting in developing a new map representing landslide susceptibility in the study area using the FR method (Figure 7). The LSM generated using the FR method categorized 26.40% of the study area as having a very low susceptibility to landslides.

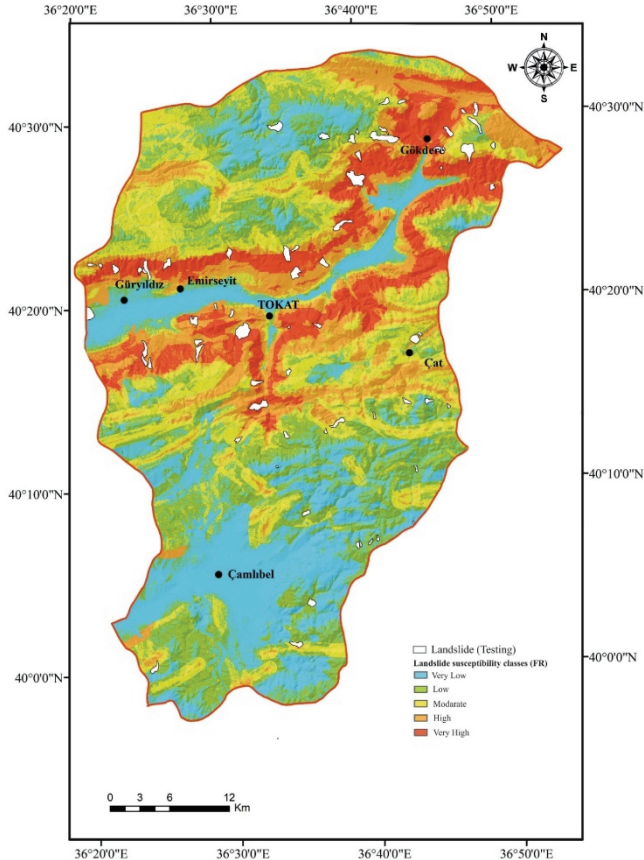


Figure 7 - Landslide susceptibility map produced by FR method

The remaining area is classified into five categories: very low, low, medium, high, and very high susceptibility. The low, medium, and high susceptibility categories cover 23.92%, 20.72%, and 16.93% of the study area, respectively. The very high susceptibility category comprises 12.03% of the total study area.

4.2. Results of the Logistic Regression Method

The present study employed the LR method as a secondary approach to generate LSMs. The LR method uses pre-existing parameter maps to create such maps. To develop the LSM via the LR method, the data of landslides and parameters obtained through the FR method were transformed into "TXT (ASCII)" format using GIS software modules. The converted data were transferred to the relevant GIS software for LR analysis and then back to raster format. Parameter data and landslide data were standardized in the range 0-1 using the "FUZZY" module and introduced into the GIS software. The data were then analyzed using the "LOGISTICREG" module in the GIS software to generate an LR equation and statistical data. The LR equation and related data are presented in Table 2. Table 2 displays the pseudo- R^2 value, which indicates the model's goodness of fit concerning the dataset in the logit model [74]. A pseudo R^2 value greater than 0.2 is considered a satisfactory match. Table 3 shows the LR equation that includes the regression coefficient and individual coefficients for each parameter to generate LSMs using the LR method.

Table 2 - Coefficients in the LR equation

Variables	Regression Coefficients
Regression Coefficient	3,8577
Aspect	3,9821
Curvature	1,5355
Distance to fault	0,5618
Distance to road	1,9804
Distance to stream	-0,2214
Elevation	-3,5103
Lithology	-1,2303
Rainfall	-0,1821
Slope	0,3579

Table 3 - Statistical summaries of the LR method

Statistics	Value
Total number of pixels	12.837.020
-2logL0	297.093,9400
-2log (possible)	162.258,7882
Goodness of fit	1.086.878,7391
Pseudo R^2	0,4538

The coefficients were aggregated using relevant modules in other GIS software to apply to previously generated parameters. The Raster Calculator was employed to create a fresh LSM, which was reclassified to obtain the final LSM of the study area using the LR method (Figure 8). The LSM generated using the LR method was categorized into five classes: very low, low, moderate, high, and very high susceptibility, similar to the FR method. The resultant LSM obtained through the LR method revealed that 28.06% of the study area was categorized as having very low susceptibility, 24.46% as having low susceptibility, 22.07% as having moderate susceptibility, 16.56% as having high susceptibility, and 8.85% as having very high susceptibility.

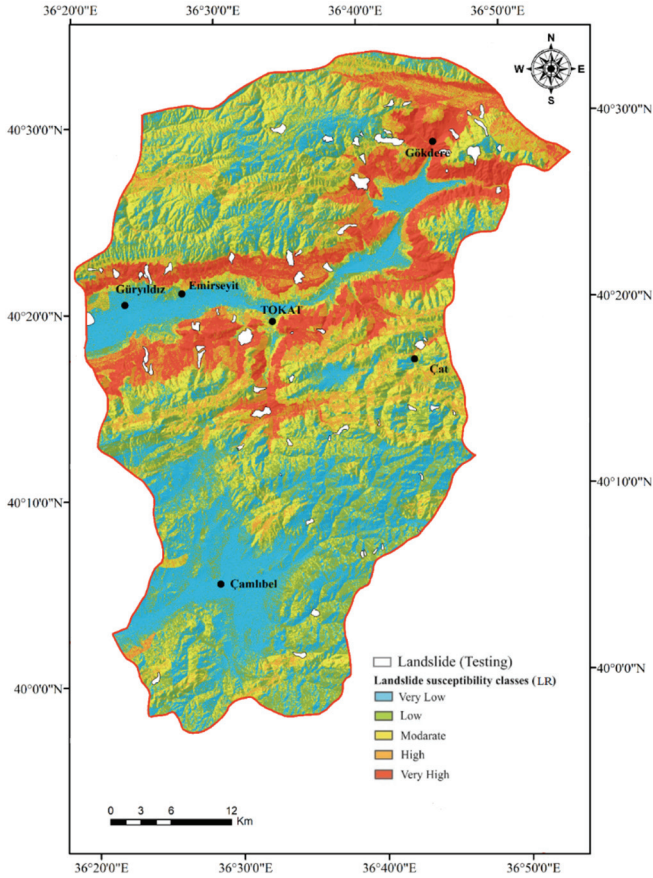
































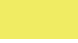




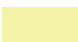





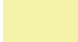









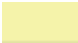




















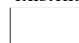


Figure 8 - Landslide susceptibility map produced by LR method

4.3. Results of Deep Learning Method

Within the scope of this study, an LSM of the study area was generated using the DNN algorithm, a DL architecture, in the final phase employing the DL method (Figure 6). The open-source ML software Weka 3.9.5 was used to execute the algorithm. The landslide and parameter map data that were employed to create LSMs through the FR and LR methods

Table 4 - Classification of landslides with the colors obtained for the parameters and the numbers assigned for analysis

PARAMETERS	FEATURES OF PARAMETERS									
Slope (°)	0-5	5-10	10-15	15-20	20-25	25-30	30-35	35-40	>40	
										
	1	2	3	4	5	6	7	8	9	
Aspect	Flat	N	NE	E	SE	S	SW	W	SW	
										
	1	2	3	4	5	6	7	8	9	
Curvature	Concave	Flat	Convex							
										
	1	2	3							
Elevation (m)	585-755	755-925	925-1080	1080-1205	1205-1310	1310-1410	1410-1535	1535-1665	1665-2079	
										
	1	2	3	4	5	6	7	8	9	
Rainfall (mm)	765-832	832-899	899-956	956-1008	1008-1115					
										
	1	2	3	4	5					
Lithology	Qal	Qym	Tmplb	Teh	Kb	Ka	Pztm	Pzt		
										
	1	2	3	4	5	6	7	8		
Distance to Faults (m)	0-100	100-200	200-300	300-400	400-500	500-600	600-700	700-800	800-900	>900
										
	1	2	3	4	5	6	7	8	9	10
Distance to Roads (m)	0-100	100-200	200-300	300-400	400-500	500-600	600-700	700-800	800-900	>900
										
	1	2	3	4	5	6	7	8	9	10
Distance to Streams (m)	0-100	100-200	200-300	300-400	400-500	500-600	600-700	700-800	800-900	>900
										
	1	2	3	4	5	6	7	8	9	10
Landslide	CLASS									
	Existent	No existent								
										
	1	0								

were also used in the DL method. To generate the LSM using the DL method, the landslide and parameter map data developed in the CBS software were initially transformed into the "TXT" format using relevant modules. The converted "TXT" data consists of a total of 12.837.020 pixels with a size of 12.5 m x 12.5 m, starting from the upper left corner of the study area and ending in the lower right corner for each parameter, including the selected 70% landslides for the application. The data were then processed in SPSS statistical software to create a dataset with each parameter's "TXT" data in a single column to be transferred to Weka for analysis. For each subparameter, numeric values ranging from 1 to 10 and class values of "1" if there is a landslide and "0" if there is no landslide were assigned to create the dataset (Table 4).

Table 5 - Classifier functions organized in the D14jMlpClassifier submodule

No	Parameters	Functions
1	layer specification	1 weka.dl4j.layers.Layer
2	Preview zoo model layer specification in GUI	False
3	number of epochs	10
4	instance integrator	Default
5	network configuration	Neural Net Configuration
6	set the iteration listener	Epoc Listener
7	zooModel	Custom Net
8	attribute normalization	Normalize training data
9	data queue size	0
10	resume	False
11	Preserve filesystem cache	False
12	batchSize	100
13	debug	False
14	doNotCheckCapalities	False
15	numDecimalPlaces	2
16	seed	1

Table 6 - Summary of DL analysis data

Summary		
Correctly Classified Examples	12.323.846	% 96.0024
Average Absolute Error	0.0727	
Mean Square Root of Errors	0.1942	
Relative Absolute Error	% 94,7029	
Relative Root Square Error	% 99,129	
Total Number of Samples	12.837.020	

The edited dataset was then transferred to Weka software to perform the DL analysis. The classifier functions of the D14jMlpClassifier sub-module were edited before DL analysis (Table 5). The software then produced the landslide susceptibility data in "TXT" format using the DL method (Table 6). The collected data underwent further processing using SPSS software before being imported into GIS software to produce an updated LSM. This newly generated map was subsequently subjected to reclassification procedures using the DL method, which divided its five distinct categories: very low, low, moderate, high, and very high susceptibility (Figure 9).

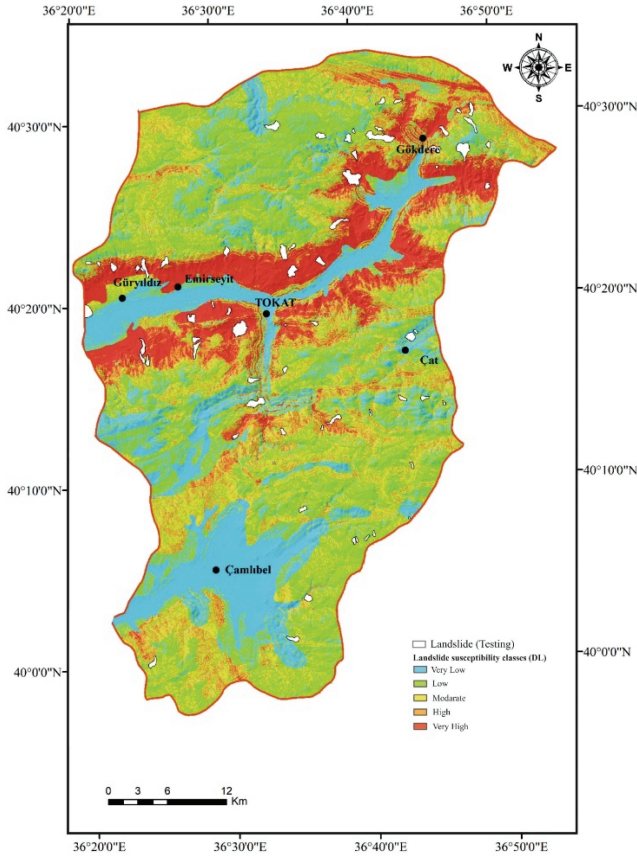


Figure 9 - Landslide susceptibility map produced by LR method

As depicted in Figure 9, the resulting susceptibility map revealed that 28.19% of the total area under study was categorized as very low susceptibility. In comparison, 34.24% was classified as low susceptibility, 20.07% as moderate susceptibility, 9.98% as high susceptibility, and 7.53% as very high susceptibility.

4.4. Performance Evaluation Methods

It has been claimed that a landslide susceptibility map (LSM) without validation lacks scientific validity, and validation's necessity in evaluating model performance has been underlined [75]. This study used the area under the receiver operating characteristic curve (AUC-ROC), overall accuracy, and precision to validate the results and compare the performance of three different methods. The performance evaluation data detailed in Table 7 are derived from the components of the confusion matrix. In Table 7, true positive (TP) and true negative (TN) indicates the number of pixels correctly classified as landslide and non-landslide, respectively, while false positive (FP) and false negative (FN) indicates the number of pixels incorrectly classified as landslide and non-landslide, respectively [76].

Table 7 - Performance assessment metrics

Metrics	Equation
ROC (AUC)	$\text{True Positive Rate (TPR)} = \frac{TP}{TP+FN}$ $\text{False Positive Rate (FPR)} = \frac{FP}{FP+TN}$
Overall Accuracy (OA %)	$OA = \frac{TP+TN}{TP+TN+FP+FN}$
Precision	$\text{Precision} = \frac{TP}{TP+FP}$

The ROC curve depicts the false positive rate (FPR) on the X-axis and the actual positive rate (TPR) on the Y-axis, illustrating the trade-off between these two rates [77]. The area under the ROC curve (AUC) is a metric for evaluating the model's predictive performance [78]. ROC curve method is based on the creation of curves on a graph through the tabulation of sensitivities and specificities for various values of a continuous test measure [79]. The values obtained from the tabulation are plotted on a coordinate plane with sensitivity (the actual positive rate) depicted on the y-axis and specificity (the false positive rate) on the x-axis to represent the ROC curve graphically. The AUC metric, the most commonly used performance evaluation metric in landslide susceptibility mapping studies, was employed in this study. Figure 7 presents the ROC curves and AUC values of the models. As illustrated in Figure 7, the DL method achieved the highest AUC value (0.858), followed by the FR (0.803) and LR (0.783) methods. Consistent with other evaluation criteria, LR lagged behind the different methods in terms of AUC (Figure 10).

Overall accuracy (OA) reflects the likelihood that a test will accurately classify an individual, calculated as the sum of true positives (TP) and true negatives (TN) divided by the total number of individuals tested. OA is the weighted average of sensitivity and specificity [80] Utilizing the performance matrix aids in determining the reliability of the classifier under evaluation. Model evaluation metrics were used during both the training and validation phases. When assessing overall accuracy (OA), it was found that the method with the lowest accuracy in both phases was logistic LR. DL demonstrated higher accuracy During the training and validation phases than the other methods.

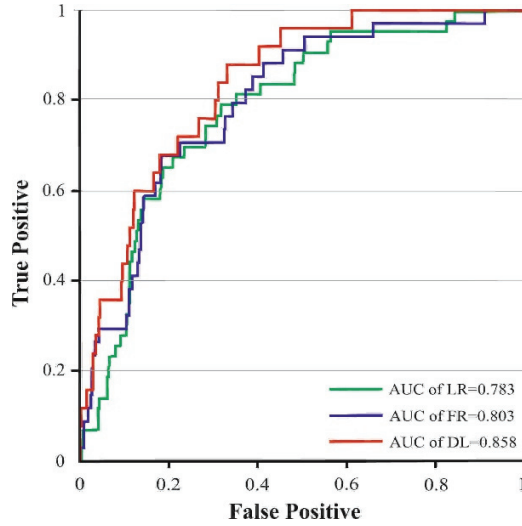


Figure 10 - ROC curves of the methods

Precision, also known as positive predictive value, is the proportion of actual positive instances among all instances identified as positive (Table 8), [81].

Table 8 - The performance of the methods applied in this study during the training and validation phase

Phase	Metrics	FR	LR	DL
Training	Accuracy (%)	81,060	80,025	84,368
	Precision	0,783	0,772	0,815
Validation	Accuracy (%)	80,329	78,811	82,340
	Precision	0,772	0,759	0,793

When the performance of the generated LSMs was evaluated, it was observed that the DL method exhibited superior sensitivity compared to the other methods. However, it is well acknowledged that the efficacy of these methods may vary depending on the specific characteristics of the study area and the conditioning factors employed.

5. CONCLUSIONS

This study applied the FR, LR, and DL methods, which are recognized as the most prevalent techniques for generating landslide susceptibility maps (LSMs), and assessed their performances. LSMs were categorized into five distinct landslide susceptibility levels. The overall accuracy, precision, and AUC-ROC metrics were employed to evaluate the validity of the generated LSMs. Across all three metric assessments, the DL method consistently

exhibited the highest performance, followed by FR and LR, respectively. Consequently, it was observed that LSMs produced by all three methods yielded satisfactory and effective results.

The outcome of the FR analysis illustrates that the category of very high susceptibility exhibits the most significant occurrence of landslides in all three maps, with subsequent classes in order of decreasing frequency being the high, moderate, low, and very low susceptibility categories. This demonstrates that the FR method effectively categorizes the study area into various landslide susceptibility classes by considering prior landslide occurrences. This implies that the method can consider previous landslide events when classifying the study area.

Furthermore, the DL method can specifically identify the features of the data through the model. For instance, in a classification problem, the features obtained manually through various methods are less likely to accurately depict the data model than the features identified by the DL method. Prior studies have indicated that the DL technique produces more accurate outcomes than other methodologies. Based on this knowledge, the outcomes of the present investigation, which were inferred from the calculated OA, precision and AUC values, imply that the LSM created by the DL approach demonstrates superior effectiveness compared to the maps generated by the FR and LR methods.

In conclusion, a comprehensive evaluation suggests that the generation of LSMs, their application in future engineering studies, and the identification of new settlements are crucial to mitigate or eliminate the detrimental effects of landslides. Additionally, developing new LSMs using various techniques and incorporating additional parameters in the map-generation process can aid in advancing scientific knowledge and the economic development of the region and country under study.

Contributions

This article is derived from the doctoral thesis titled “TOKAT İL MERKEZİNİN HEYELAN DUYARLILIK ANALİZİ” (<https://tez.yok.gov.tr/UlusalTezMerkezi/tezSorguSonucYeni.jsp-761579>).

References

- [1] Hungr, O., Leroueil, S., Picarelli, L., The Varnes classification of landslide types, an update. *Landslides*, 11, 167-194, 2014.
- [2] Jakob, M., Chapter 14 - Landslides in a changing climate, *Landslide Hazards, Risks, and Disasters (Second Edition)*. Hazards and Disasters Series, 505-579, 2022.
- [3] AFAD, *Landslide-Rockfall Basic Guide*. Ministry of Interior Disaster and Emergency Management Presidency, Ankara, Turkey, 2018.
- [4] Yalcin, A., Reis, S., Aydinoglu, A.C., Nadirli, S.A., A GIS-based comparative study of frequency ratio, analytical hierarchy process, bivariate statistics, and logistics regression methods for landslide susceptibility mapping in Trabzon, NE Turkey. *Catena*, 2011.

- [5] Guzzetti, F., Mondini, A.C., Cardinali, M., Fiorucci, F., Landslide inventory maps: New tools for an old problem. *Earth-Science Reviews*, 112, 42-66, 21, 2012.
- [6] Bhandari, B.P., Dhakal, S., Topographical and geological factors on gully-type debris flow in Malai River catchment, Siwaliks, Nepal. *Journal of Nepal Geological Society*, 59, 2019.
- [7] Gariano, S.L., Melillo, M., Peruccacci, S., How much does the rainfall temporal resolution affect rainfall thresholds for landslide triggering? *Natural Hazards*, 100, 655-670, 2020.
- [8] Kumi-Boateng, B., Peprah, M.S., Larbi, E.K., Prioritization of forest fire hazard risk simulation using hybrid grey relativity analysis (HGRA) and fuzzy analytical hierarchy process (FAHP) coupled with multicriteria decision analysis (MCDA) techniques - a comparative study analysis. *Geodesy and Cartography* 47, 3, 2021.
- [9] Wubalem, A., Landslide Inventory, Susceptibility, Hazard and Risk Mapping. Submitted: June 25th, 2021 Reviewed: September 17th, 2021 Published: November 20th, 2021.
- [10] Shano, L., Raghuvanshi, T.K., Meten, M., Landslide susceptibility evaluation and hazard zonation techniques - a review. *Geoenvironmental Disasters*, 7, 18, 2020.
- [11] Turan, I.D., Ozkan, B., Turkes, M., Deniz, O., Landslide susceptibility mapping for the Black Sea Region with spatial fuzzy multi-criteria decision analysis under semi-humid and humid terrestrial ecosystems. *Theoretical and Applied Climatology*, 140, 1233-1246, 2020.
- [12] Marker, B.R., Hazard and Risk Mapping, First Online: 01 January 2016, Citations Part of the Encyclopedia of Earth Sciences Series book series (EESS), 2016.
- [13] Reichenbach, P., Rossi, M., Malamud, B.D., Mihir, M., Guzzetti, F., A review of statistically-based landslide susceptibility models. *Earth-Science Reviews* 180, 60-91, 2018.
- [14] Pradhan, B., A comparative study on the predictive ability of the decision tree, support vector machine, and neuro-fuzzy models in landslide susceptibility mapping using GIS. *Computer and Geosciences*, 51, 350-365, 2013.
- [15] Chen, T., Niu, R., Du, B., Landslide spatial susceptibility mapping using GIS and remote sensing techniques: a case study in Zigui County, the Three Georges reservoir, China. *Environmental Earth Sciences*, 73, 5571-5583, 2015.
- [16] Saleem, N., Huq, E., Twumasi, N.Y.D., Javed, A., Sajjad, A., Parameters Derived from and/or Used with Digital Elevation Models (DEMs) for Landslide Susceptibility Mapping and Landslide Risk Assessment: A Review. *Geospatial Approaches to Landslide Mapping and Monitoring*, 8, 545, 2019.
- [17] Pourghasemi, H.R., Yansari, Z.T., Panagos, P., Pradhan, B., Analysis and evaluation of landslide susceptibility: a review of articles published during 2005-2016 (periods of 2005-2012 and 2013-2016). *Arabian Journal of Geosciences*, 11, 193, 2018.

- [18] Bui, D.T., Tuan, T.A., Klempe, H., Pradhan, B., Revhaug, I., Spatial prediction models for shallow landslide hazards: a comparative assessment of the efficacy of support vector machines, artificial neural networks, kernel logistic regression, and logistic model tree. *Landslides*, 13, 361-378, 2016.
- [19] Yong, C., Jinlong, D., Fei, G., Bin, T., Tao, Z., Hao, F., Li, W., Qinghua, Z., Review of landslide susceptibility assessment based on knowledge mapping. *Stochastic Environmental Research and Risk Assessment*, 36, 2399-2417, 2022.
- [20] NVİ, Tokat Provincial Directorate of Population and Citizenship, Tokat, Turkey, 2022.
- [21] Ayele, S., Raghuvanshi, T.K., Kala, P.M., Application of Remote Sensing and GIS for Landslide Disaster Management: A Case from Abay Gorge, Gohatsion–Dejen Section, Ethiopia. *Landscape Ecology and Water Management*, 15-32, 2014.
- [22] Althuwaynee, O.F., Pradhan, B., Park, H.J., Lee, J.H., A novel ensemble bivariate statistical evidential belief function with knowledge-based analytical hierarchy process and multivariate statistical logistic regression for landslide susceptibility mapping. *Catena*, 114, 21-36, 2014.
- [23] Chen, W., Xie, X., Peng, J., Shahabi, H., Hong, H., Bui, D.T., Duan, Z., Li, S., Zhu, A., GIS-based landslide susceptibility evaluation using a novel hybrid integration approach of bivariate statistical based random forest method. *Catena*, 164, 135-149, 2018.
- [24] Lee, S., Current and Future Status of GIS-based Landslide Susceptibility Mapping: A Literature Review. *Korean Journal of Remote Sensing*, 1, 179-193, 2019.
- [25] Meng, Q., Miao, F., Zhen, J., Wang, X., Wang, A., Peng, Y., Fan, Q., GIS-based landslide susceptibility mapping with logistic regression, analytical hierarchy process, and combined fuzzy and support vector machine methods: a case study from Wolong Giant Panda Natural Reserve, China. *Bulletin of Engineering Geology and the Environment*, 75, 923-944, 2016.
- [26] Kavzoglu, T., Teke, A., Predictive Performances of Ensemble Machine Learning Algorithms in Landslide Susceptibility Mapping Using Random Forest, Extreme Gradient Boosting (XGBoost) and Natural Gradient Boosting (NGBoost). *Arabian Journal for Science and Engineering*, 47, 7367-7385, 2022.
- [27] Zhang, H., Song, Y., Xu, S., He, Y., Li, Z., Yu, X., Liang, Y., Wu, W., Wang, Y., Combining a class-weighted algorithm and machine learning models in landslide susceptibility mapping: A case study of Wanzhou section of the Three Gorges Reservoir, China. *Computer and Geosciences*, 158, 2022.
- [28] Chung, C.F., Fabbri, A.G., Validation of spatial prediction models for landslide hazard mapping. *Natural Hazards*, 30, 451-472, 2003.
- [29] Ohlmacher, G.C., Davis, J.C., Using multiple logistic regression and GIS technology to predict landslide hazard in northeast Kansas, USA. *Engineering Geology*, 69, 3-4, 331-343, 2003.
- [30] Nachappa, T.G., Kienberger, S., Meeana, S.R., Hölbling, D., Blaschke, T., Comparison and validation of per-pixel and object-based approaches for landslide susceptibility mapping. *Geomatics, Natural Hazards and Risk*, 572-600, 2020.

- [31] Ercanoglu, M., Gokceoglu, C., Use of fuzzy relations to produce landslide susceptibility map of a landslide prone area (West Black Sea Region, Turkey). *Engineering Geology*, 75:229-250, 2004.
- [32] MTA, General Directorate of Mineral Research and Exploration, Ankara, Turkey, 2020.
- [33] Tsangaratos, P., Ilia, I., Comparison of logistic regression and Naïve Bayes classifier in landslide susceptibility assessments: The influence of models complexity and training dataset size. *Catena*, 145, 164-179, 2016.
- [34] Sun, D., Wen, H., Wang, D., Xu, J., A random forest model of landslide susceptibility mapping based on hyperparameter optimization using Bayes algorithm. *Geomorphology*, 362, 2020.
- [35] Conforti, M., Letto, F., Modeling Shallow Landslide Susceptibility and Assessment of the Relative Importance of Predisposing Factors, through a GIS-Based Statistical Analysis. *Geosciences*, 11, 8, 2021.
- [36] Siddique, T., Pradhan, S.P., Stability and sensitivity analysis of Himalayan road cut debris slopes: an investigation along NH-58, India. *Natural Hazards*, 93, 577-600, 2018.
- [37] El-Magd, S.A.A., Eldosouky, A.M., An improved approach for predicting the groundwater potentiality in the low desert lands; El-Marashda area, Northwest Qena City, Egypt. *Journal of African Earth Sciences*, 179, 2021.
- [38] Qin, Z., Lai, Y., Tian, Y., Study on failure mechanism of a plain irrigation reservoir soil bank slope under wind wave erosion. *Natural Hazards*, 109, 567-592, 2021.
- [39] Akgun, A., GIS-based erosion and landslide susceptibility assessment of the Ayvalık and surroundings. Ph.D. Thesis, Dokuz Eylül University, İzmir, Turkey, 2007.
- [40] Dai, F.C., Lee, C.F., Landslide characteristics and slope instability modeling using GIS. Lantau Island, Hong Kong. *Geomorphology*, 42, 213-228, 2002.
- [41] Liu, Q., Tang, A., Exploring aspects affecting the predicted capacity of landslide susceptibility based on machine learning technology. *Geocarto International*, 14547-14569, 2022.
- [42] Gokceoglu, C., Sonmez, H., Nefeslioglu, H.A., Duman, T.Y., Can, T., The 17 March 2005 Kuzulu landslide (Sivas, Turkey) and landslide-susceptibility map of its near vicinity. *Engineering Geology*, 81, 1, 65-83, 2005.
- [43] Duman, T.Y., Can, T., Gokceoglu, C., Application of logistic regression for landslide susceptibility zoning of Cekmece Area, Istanbul, Turkey. *Environmental Geology*, 51, 241-256, 2006.
- [44] Gokceoglu, C., Ercanoglu, M., Uncertainties on the parameters employed to prepare landslide susceptibility maps. *Bulletin of Earth Sciences Application and Research Centre of Hacettepe University Critical Review*, 2001.
- [45] Terranova, O.G., Garaino, S.L., Bruno, C., Greco, R., Pellegrino, A.D., Iovine, G.G.R., Landslide-risk scenario of the Costa Viola mountain ridge (Calabria, Southern Italy). *Journal of Maps*, 12, 261-270, 2016.

- [46] Clerici, A., Perego, S., Vescovi, P., A procedure for landslide susceptibility zonation by the conditional analysis method. *Geomorphology*, 48 (4): 349-364, 2002.
- [47] Ayalew, L., Yamagishi, H., The application of GIS-based logistic regression for landslide susceptibility mapping in the Kakuda-Yahiko Mountains (Central Japan). *Geomorphology*, 65, 15-31, 2005.
- [48] Ermini, L., Catani, F., Casagli, N., Artificial Neural Networks applied to landslide susceptibility assessment. *Geomorphology*, 66, 327-343, 2005.
- [49] Luzi, L., Pergalani, F., Slope Instability in Static and Dynamic Conditions for Urban Planning: the 'Oltre Po Pavese' Case History (Regione Lombardia- Italy), *Natural Hazards*, 20, 57-82, 1999.
- [50] Wachal, D.J., Hudak, P.F., Mapping landslide susceptibility in Travis County. Texas, USA, *GeoJournal*, 51, 245-253, 2000.
- [51] Siahkamari, S., Haghizadeh, A., Zeinivand, H., Tahmasebipour, N., Rahmati, O., Spatial prediction of flood-susceptible areas using frequency ratio and maximum entropy models. *Geocarto International*, 33, 927-941, 2017.
- [52] Huang, F., Yao, C., Liu, W., Li, Y., Liu, X., Landslide susceptibility assessment in the Nantian area of China: a comparison of frequency ratio model and support vector machine. *Geomatics, Natural Hazards and Risk*, 9, 919-938, 2018.
- [53] Khan, H., Shafique, M., Khan, M.A., Bacha, M.A., Shah, S.U., Calligaris, C., Landslide susceptibility assessment using Frequency Ratio, a case study of northern Pakistan. *The Egyptian Journal of Remote Sensing and Space Sciences*, 22, 11-24, 2018.
- [54] Gholami, M., Ghachkanlu, M.E., Khosravi, K., Pirasteh, S., Landslide prediction capability by comparison of frequency ratio, fuzzy gamma and landslide index method. *Journal of Earth System Sciences*, 128, 42, 2019.
- [55] Lee, S., Ryu, J., Won, J., Park, H., Determination and application of the weight for landslide susceptibility mapping using an artificial neural network. *Engineering Geology*, 71-80, 2004.
- [56] Ataol, M., Yesilyurt, S., Identification of landslide risk zones along the Çankırı-Ankara (Between Akyurt and Çankırı) state road. *Journal of Geography*, 0, 51-69, 2014.
- [57] Pham, B.T., Bui, D.T., Indra, P., Dholakia, M., Landslide Susceptibility Assessment at a Part of Uttarakhand Himalaya, India using GIS-based Statistical Approach of Frequency Ratio Method. *International Journal of Engineering Research and Technology*, 11, 338-344, 2015.
- [58] Demir, G., GIS-Based Landslide Susceptibility Mapping for a Part of the North Anatolian Fault Zone between Reşadiye and Koyulhisar (Turkey). *Catena*, 183, 104211, 2019.
- [59] Silalahi, F.E.S., Arifianti, P.Y., Hidayat, F., Landslide susceptibility assessment using frequency ratio model in Bogor. West Java, Indonesia. *Geoscience Letter*, 6, 10, 2019.

- [60] Erener, A., Lacasse, S., Landslide susceptibility mapping using GIS, 28th Asian Conference on Remote Sensing, 2007, Kuala Lumpur, Malaysia, 2007.
- [61] Demir, G., Landslide Susceptibility Mapping by Using Statistical Analysis in the North Anatolian Fault Zone (NAFZ) on the Northern Part of Suşehri Town, Turkey. *Natural Hazard*, 92, 133-154, 2018.
- [62] Karaman, M.O., Cabuk, S.N., Pekkan, E., Utilization of Frequency Ratio Method for the Development of Landslide Susceptibility Maps: Karaburun Peninsula Case, Turkey. *Research Square*, 2022.
- [63] Hilbe, J.M., *Logistic Regression Models*. 1st edition, New York, 2009.
- [64] Kleinbaum D.G., Kupper, L.L., Muller, K.E., *Applied regression analysis and other multivariable methods*. 3rd Edition, Duxbury Press, California, 798, 1998.
- [65] Atkinson, P.M., Massari, R., *Generalized Linear Modelling of Susceptibility to Attributes*. *Engineering Geology*, 32, 81-100, 1998.
- [66] Bui, D.T., Lofman, O., Revhaug, I., Landslide susceptibility analysis in the Hoa Binh province of Vietnam using statistical index and logistic regression. *Natural Hazards*, 59, 1413-144, 2011.
- [67] Das, I., Sahoo, S., van Westen, C., Stein, A., Haçık, R., Landslide susceptibility assessment using logistic regression and its comparison with a rock mass classification system, along a road section in the northern Himalayas (India). *Geomorphology*, 114, 1, 627-637, 2010.
- [68] Lang, S., Marquez, F.M., Beckham, C., Hall, M., Frank, E., WekaDeepLearning4j: A deep learning package for Weka based on DeepLearning4j. *Knowledge-Based Systems*, 178, 48-50, 2019.
- [69] Bengio, Y., *Deep learning of representations: looking forward*, Part of the Lecture Notes in Computer Science Book Series. Montreal University, Canada, 1-2, 2013.
- [70] LeCun, Y., Bengio, Y., Hinton, G., *Deep learning*. *Nature*, 521, 436-444, 2015.
- [71] Schmidhuber, J., *Deep learning in neural networks: An overview*. *Neural Networks*, 61, 85-117, 2015.
- [72] Goodfellow, I., Bengio, Y., Courville, A., *Deep learning*. MIT Press, 2016.
- [73] Jordan, M.I., Mitchell, T.M., *Machine learning: Trends, perspectives, and prospects*. *Science*, 349, 255-260, 2015.
- [74] Clark, W.A.V., Hosking, P.L., *Statistical Methods for Geographers*, John Wiley and Sons. 518, New York, 1991.
- [75] Akinci, H.A., Akinci, H., *Machine learning based forest fire susceptibility assessment of Manavgat district (Antalya)*. *Turkey Earth Science Informatics*, 16(1):397-414, 2023.

- [76] Ye, P., Yu, B., Chen, W., Liu, K., Ye, L., Rainfall-induced landslide susceptibility mapping using machine learning algorithms and comparison of their performance in Hilly area of Fujian Province. *China Nat. Hazards*, 113:965-995, 2022.
- [77] Pourghasemi, H.R., Pradhan, B., Gokceoglu, C., Moezzi, K.D., Landslide susceptibility mapping using a spatial multi criteria evaluation model at Haraz watershed, Iran. In *Terrigenous Mass Movements*; Pradhan, B., Buchroithner, M., Eds.; Springer: Berlin/Heidelberg, Germany, pp. 23-49. ISBN 978-3-642-25495-6, 2012.
- [78] Yilmaz, I., Landslide susceptibility mapping using frequency ratio, logistic regression, artificial neural networks and their comparison: A case study from Kat landslides (Tokat-Turkey). *Comput Geosci* 35(6):1125–1138, 2009.
- [79] Hoo, H.Z, Candlish, J., Teare, D., What is an ROC curve? *Emergency Medicine Journal*, 34, 6, 2017.
- [80] Aggarwal, C. C., *Neural Networks and Deep Learning*, Vol. 497, Springer, 2018.
- [81] Azarafza, M., Akgun, H., Atkinson, P.M., Derakhshani, R., Deep learning-based landslide susceptibility mapping. *Sci Rep* 11:24112, 2021.